Radar Vertical Profile of Reflectivity Correction with TRMM Observations Using a Neural Network Approach

YADONG WANG

Cooperative Institute for Mesoscale Meteorological Studies, University of Oklahoma, and NOAA/OAR/National Severe Storms Laboratory, Norman, Oklahoma

JIAN ZHANG

NOAA/OAR/National Severe Storms Laboratory, Norman, Oklahoma

PAO-LIANG CHANG

Central Weather Bureau, Taipei, Taiwan

QING CAO

Enterprise Electronics Corporation, Enterprise, Alabama

(Manuscript received 11 July 2014, in final form 15 May 2015)

ABSTRACT

Complex terrain poses challenges to the ground-based radar quantitative precipitation estimation (QPE) because of partial or total blockages of radar beams in the lower tilts. Reflectivities from higher tilts are often used in the QPE under these circumstances and biases are then introduced due to vertical variations of reflectivity. The spaceborne Precipitation Radar (PR) on board the Tropical Rainfall Measuring Mission (TRMM) satellite can provide good measurements of the vertical structure of reflectivity even in complex terrain, but the poor temporal resolution of TRMM PR data limits their usefulness in real-time QPE. This study proposes a novel vertical profile of reflectivity (VPR) correction approach to enhance ground radar–based QPEs in complex terrain by integrating the spaceborne radar observations. In the current study, climatological relationships between VPRs from an S-band Doppler weather radar located on the east coast of Taiwan and the TRMM PR are developed using an artificial neural network (ANN). When a lower tilt of the ground radar is blocked, higher-tilt reflectivity data are corrected with the trained ANN and then applied in the rainfall estimation. The proposed algorithm was evaluated with three typhoon precipitation events, and its preliminary performance was evaluated and analyzed.

1. Introduction

In the ground radar quantitative precipitation estimation (QPE), data from the lowest tilt are preferred since they usually incur minimal errors because of 1) changes of radar variables with height and 2) horizontal drifts of hydrometeors as they fall from the height of the radar resolution volume to the ground (Zrnić and Ryzhkov 1996). The radar-based QPE in Taiwan suffers from severe beam blockages due to the complex terrain of the Central Mountain Range (CMR), which peaks at nearly 4000 m above mean sea level (MSL; Fig. 1). When a radar beam in the lowest tilt is completely blocked, higher-tilt data are usually used in the QPE. However, when hydrometeors descend from the radar observation height to the ground, various microphysics processes (e.g., melting, aggregation, breakup, collision, coalescence, and evaporation) could cause reflectivity variations with height. The nonuniform vertical structure of reflectivity often results in a bias in the radar-based QPE (e.g., Andrieu and Creutin 1995; Marzano et al. 2004) when compared with surface gauge observations.

Corresponding author address: Yadong Wang, CIMMS, University of Oklahoma, 120 David L. Boren Blvd., Norman, OK 73072.
E-mail: yadong.wang@noaa.gov

DOI: 10.1175/JHM-D-14-0136.1

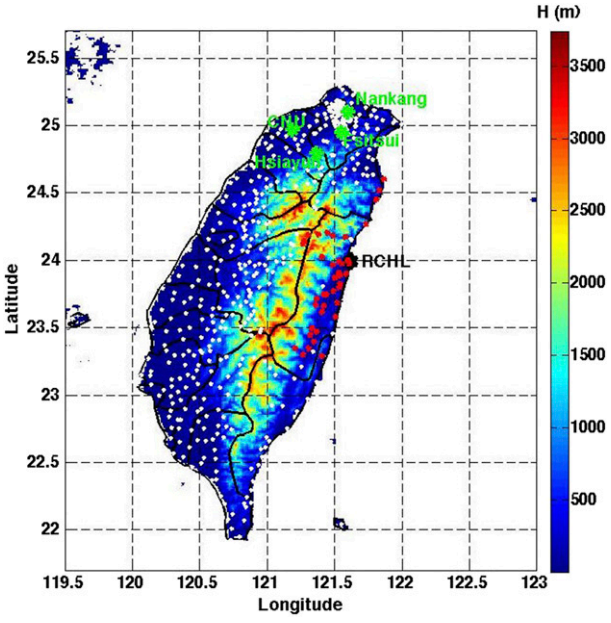

FIG. 1. The terrain map of Taiwan, where color shows the heights of the CMR. The location of an S-band radar (RCHL) used in the current work is indicated by a black square, and the location of each gauge is indicated by a white dot. The reflectivity–rain rate relations are derived using the observations from four impact-type JWDs, and their locations are indicated by green stars. The gauges used in the performance evaluation are marked as red dots.

To mitigate the ground radar QPE bias associated with the nonuniform reflectivity structure, many vertical profile of reflectivity (VPR) correction approaches have been developed. A VPR correction extrapolates high-altitude radar data to a lower reference height based on a priori reference VPR (e.g., Andrieu and Creutin 1995; Fabry and Zawadzki 1995; Rico-Ramirez et al. 2005, 2007; Zhang et al. 2008; Zhang and Qi 2010; Qi et al. 2013). For any VPR correction method, determining a representative reference VPR is the first and most important step. Reference VPRs could be derived from physical models or from radar observations in a nearby area or a similar climatology region where the radar is not blocked. The reference VPR is usually averaged over a certain spatial and temporal domain (e.g., Joss and Waldvogel 1970; Harrold and Kitchingam 1975; Willis and Heymsfield 1989; Kitchen 1997; Smyth and Illingworth 1998; Zhang et al. 2008; Zhang and Qi 2010). For the Hua-Lian radar (RCHL) located on the east coast of Taiwan (Fig. 1), the terrain rises sharply from 0 to 2500 m MSL within 15 km and causes severe blockages (100% to all tilts below the 2.4° elevation angle) in the western half of the radar umbrella. While data from the eastern half of the radar umbrella could be used to calculate VPRs that extend down to lower altitudes near the ground, they are from the ocean region and may be significantly different from those over the steep terrain where orographic precipitation enhancements are often present.

The Tropical Rainfall Measuring Mission (TRMM) is a satellite-based program that provided global-range tropical rainfall estimation since it was launched in November 1997. As the world's foremost satellite designed for precipitation measurement, TRMM is under the joint operation by the National Aeronautics and Space Administration (NASA) and the Japan Aerospace Exploration Agency (JAXA). Compared to ground-based weather radars, TRMM's Ku-band Precipitation Radar (PR) has two major advantages: 1) TRMM PR can provide reflectivity data with a fine vertical resolution of 250 m, while the beamwidth of S-band radars such as RCHL could reach a few kilometers at far range, and 2) compared to a ground-based radar, TRMM PR can provide better observations on the vertical structure of reflectivity, especially in complex terrain regions, where a lower-tilt ground-based radar beam is totally blocked. On the other hand, ground-based radar observations have a very high temporal resolution of approximately 5–10 min while the number of TRMM overpasses is only about one every other day. The poor temporal resolution significantly limits the use of TRMM PR in real-time precipitation estimation.

In the current study, a new radar VPR correction approach with TRMM PR observations was developed. Reflectivity fields observed by RCHL and TRMM PR from the same time and location are collected and relationships between VPRs of the two sensors are developed through an artificial neural network (ANN). The trained ANN is then used to retrieve lower-altitude radar reflectivities from the unblocked higher-tilt data in areas of severe beam blockages and the retrieved reflectivity is applied in the rain-rate estimation. The proposed approach was evaluated for three typhoon events with surface gauge observations.

This paper is organized as follows. Section 2 describes the data and its processing. The ANN VPR correction scheme is introduced in section 3 and its performance is evaluated in section 4. A summary is provided in section 5.

2. Data sources and processing

a. The impact of complex terrain on radar reflectivity

A Gematronik 1500S Doppler radar (RCHL) located at 23.99°N, 121.62°E (Fig. 1) is the main data source for the real-time radar QPE and flood warnings in the east coastal area of Taiwan. The key system characteristics of

RCHL are listed in Table 1. Since RCHL is within 20 km of the steep slopes on the east side of the CMR, the two lowest tilts (0.5° and 1.4°) are completely blocked (Figs. 2a,b) to the west of the radar. There are even some small blockages at the 9.9° elevation angle (Fig. 2e). To the east of the radar is the Pacific Ocean, and all tilts are unblocked. To the west of the radar, heights of the lowest unblocked beams (Fig. 3) quickly change from 0.2 to 4.0 km on the east side of the CMR and shoot above 5 km beyond the ridge of CMR. While other radars in Taiwan provide better coverage on the west side of CMR, RCHL is the main radar for the east coastal areas, even though the lower-level coverage is very limited.

Figure 4 shows example reflectivity fields from Typhoon Tembin at 0945 UTC 23 August 2012, where the typhoon eye can be identified at approximately 22.5°N, 122.75°E. The lowest two tilts (0.5° and 1.4°) did not provide any data over the island of Taiwan because of the severe blockage. The 4.3° (Fig. 4c) and 6.0° (Fig. 4d) tilts provide small coverage over the east coast of Taiwan, although the reflectivities were apparently weaker than those in the lower tilts. For instance, the mean reflectivities within the black dashed circles from these four tilts are 29, 27, 19, and 13 dBZ, respectively. If reflectivities from the 4.3° or 6.0° elevation angles are used for the rain-rate estimation without any vertical correction, significant underestimation may be introduced.

To obtain reliable QPEs in complex terrain, various approaches using gauge data have been developed. Such approaches include the real-time local gauge bias correction of radar QPE (e.g., Germann and Joss 2002; Goudenhoofdt and Delobbe 2009) and gauge and orographic precipitation climatology combined QPE (Schaake et al. 2004; Daly et al. 1994). In addition, the quality of a gauge-based QPE is highly dependent on the density of the gauge network. The density of the gauge network along the east coast of Taiwan is apparently lower than in the west plains region (Fig. 1), and such gauge density would not be able to capture the highly variable orographic rain in this complex terrain. Therefore, a radar-based QPE is still needed.

b. *The reflectivity field observed by TRMM*

The TRMM PR operates at Ku band with a frequency of 13.8 GHz (Kozu et al. 2001; Kummerow et al. 2000) and scans across a 215-km-wide swath with vertical and horizontal resolutions at nadir of 250 m and 4.3 km, respectively. There are three levels of radar algorithms developed for TRMM PR products: the basic radar parameters such as return power and radar reflectivity Z (from the level I algorithm), products associated with radar signal processing and physical process of storms (from the level II algorithm), and space–time averaging and statistics products of level I and II (from the level III algorithm; Cao et al. 2013a). The datasets used in this example were generated by the level II algorithm of the PR profile algorithm (2A25), which provides range profiles of attenuation-corrected and ground-clutter-filtered radar reflectivity and the corresponding rainfall estimation (Meneghini et al. 2000, 2004; Iguchi et al. 2000, 2009). Wen et al. (2013) applied a physically based VPR model proposed by Kirstetter et al. (2010) to correct the vertical variations in radar reflectivity. However, model errors attributed to the assumption of icing and melting processes, as well as the shape of VPR, have not be fully studied (Cao et al. 2013b).

TABLE 1. Technical specifications of the Gematronik 1500S Doppler radar (RCHL) used in the current work.

	Specifications
Pulse peak power	750 kW
Frequency range	2.7–2.9 GHz
Pulse length	0.53 μs
Range resolution	0.25 km
Beamwidth	1°
Antenna diameter	8.6 m
PRF	250–1300 Hz
Lat	23.990°N
Lon	121.6200°E
Radar height	63 m
Elev angle	0.5°, 1.4°, 2.4°, 3.4°, 4.3°, 6.0°, 9.9°, 14.6°, 19.5°

While TRMM PR provides good reflectivity observations, the data cannot be directly utilized in real-time QPE because of the low frequency for any given location, especially for the Taiwan area. For example, during the 5-day period between 8 and 12 August 2009 (Typhoon Morakot), TRMM only passed through the Taiwan region five times, as shown in Fig. 5. Among them, only the swath at 2042 UTC 8 August 2009 covered most parts of Taiwan while others covered small parts of the island.

3. VPR correction with an ANN approach

Artificial neural network has been applied in weather radar applications for purposes of precipitation forecasting, rain-rate estimation, damaging wind prediction, cloud classification, radar data quality control, etc. (e.g., Bankert and Aha 1996; Marzban and Stumpf 1998; Hall et al. 1999; Orlandini and Morlini 2000; Lakshmanan et al. 2007; Roebber et al. 2007). Different from physically based approaches where a priori knowledge or assumptions are needed, ANN does not require a priori physical rules and handles complex problems that are not well understood with statistical constraints. An

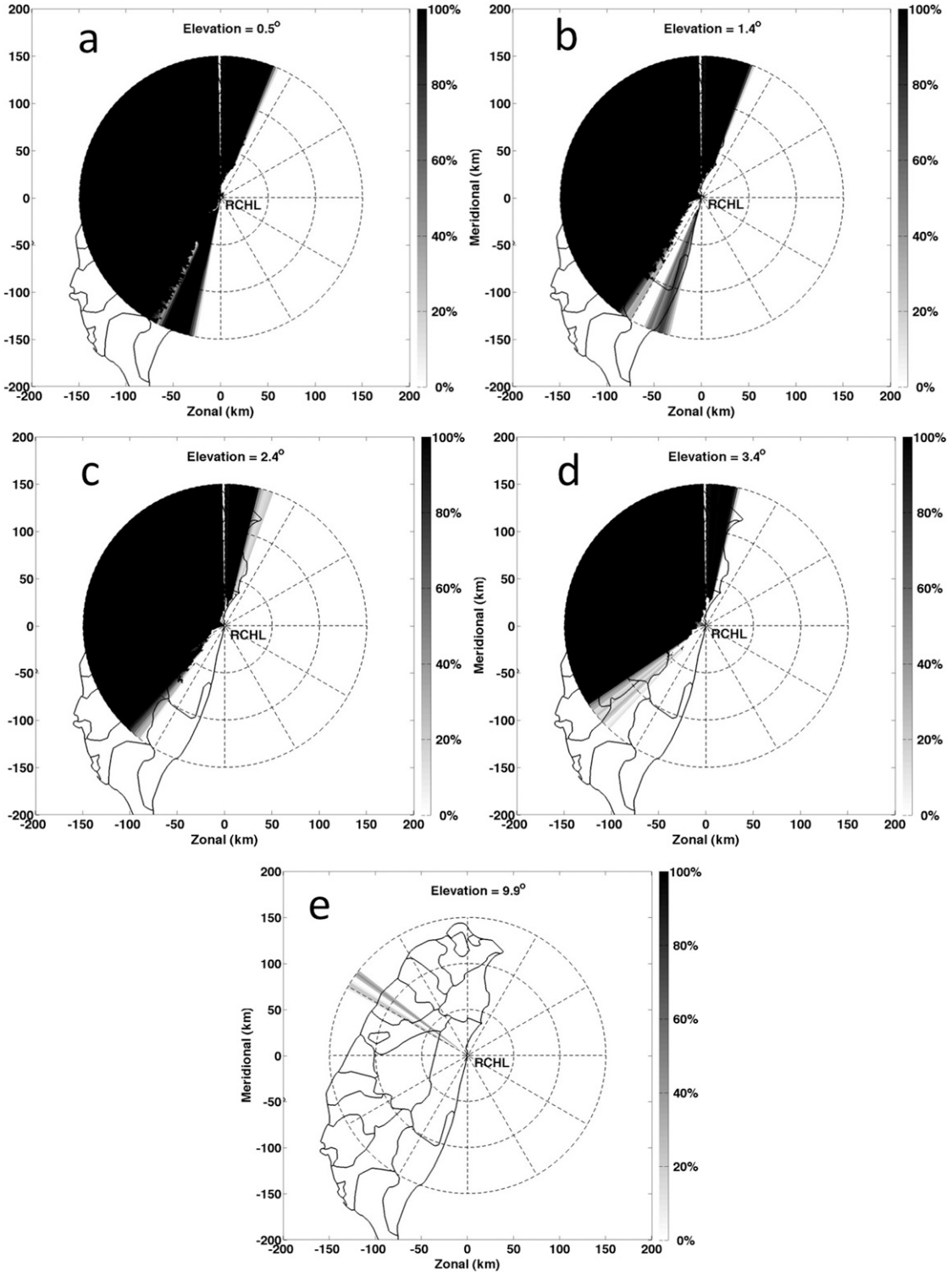

FIG. 2. Radar beam blockage percentages from elevation angles of (a) 0.5°, (b) 1.4°, (c) 2.4°, (d) 3.4°, and (e) 9.9°. The gray map indicates the blockage percentage.

ANN-based VPR correction approach was developed by Marzano et al. (2004) for a C-band meteorological radar located in central Italy, in which a reference VPR was obtained by training an ANN with volumetric data collected from close range (within 60 km), where both the near-surface and high-altitude reflectivities are available. The ANN-based VPR correction was applied to radar data at far ranges and produced improved rain-rate estimation (Marzano et al. 2004) over the data without the correction. This approach cannot be applied to RCHL over the western half of the radar domain because of a lack of lower-tilt data for ANN training. The ANN approach was tested using data from the east side of the radar, but the derived VPRs did not provide significant improvements for the radar QPE to the west because the VPR characteristics were different over the ocean (east of the radar) than over the land. Detailed discussions of VPRs sampled from land and ocean regions are provided in section 4. It should be noted that the precipitation could be estimated with ANN approaches using gauge observations (e.g., Hall et al. 1999; Hung et al. 2009; Luk et al. 2001), but the current work focuses on the radar-based QPE and will not discuss ANN approaches from gauge observations.

A new ANN approach was developed in the current study, where the ANN was trained using the combination of TRMM PR data and radar data instead of the radar data only. The new ANN VPR correction algorithm utilizes a feed-forward ANN as shown in Fig. 6, which includes a linear least squares simplex algorithm to search for the optimal input–output relations in the training process (Hsu et al. 1995). The ANN consists of two layers of neural nodes, which are connected by a weighting summation and extra adjusting factors. The nodes (20 nodes) in the hidden layer combine the input values using an operation of weighting summation as shown in Eq. (1), where $\mathbf{X}$ is the input vector, $\mathbf{W}_{W,N}$ is the trained matrix, and b^1 is the adjusting factor. The number of input variables and nodes are denoted with W and N. The outputs are calculated with a logistic sigmoid activation function, as shown in Eq. (2), where $a = \mathbf{W}^1_{W,N}\mathbf{X} + b^1$:

$$O_H = f(\mathbf{W}^1_{W,N}\mathbf{X} + b^1) \tag{1}$$

where

$$f(a) = \frac{1}{1 + \exp(-a)}. \tag{2}$$

Similarly, the output layer calculates the final output of x_1 and x_2 using the outputs of the hidden layer and a trained matrix $\mathbf{W}^2_{W,N}$ and adjusting factor b^2 using Eqs. (1) and (2).

The input variables of the ANN are the normalized radar reflectivities from three adjacent higher tilts, and

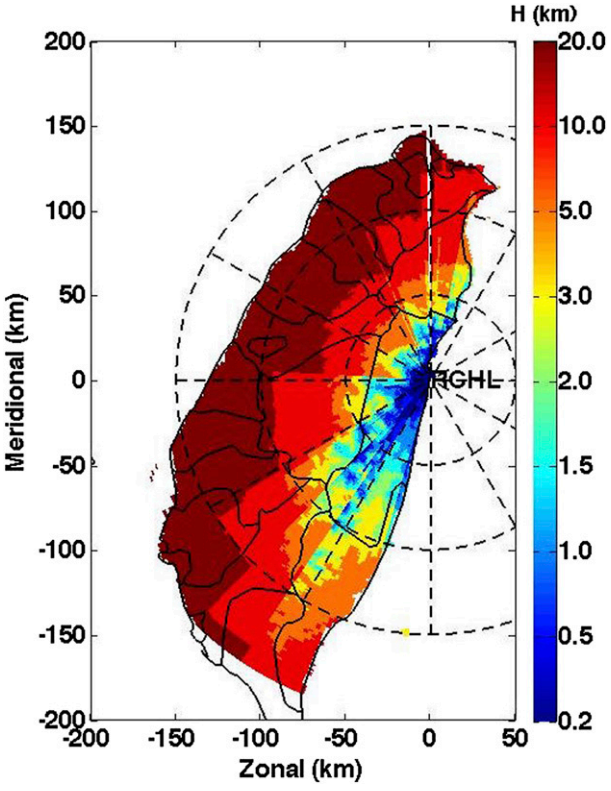

FIG. 3. The distance between the center of the lowest unblocked beams and the ground surface.

the outputs are the normalized radar reflectivities at the two lowest tilts. The reference height of normalization is 5 km MSL, which is the approximate height of the melting layer bottom. Generally, the ground level is selected as the reference height in the VPR normalization (e.g., Andrieu and Creutin 1995); however, the ground level is varied in the mountain region and the maximum difference could reach 3000 m. Therefore, the height of the melting layer bottom is selected as the reference height, which is relatively more stable than the ground level.

The weighting matrices ($\mathbf{W}^1_{W,N}$ and $\mathbf{W}^2_{W,N}$) and the adjusting factors (b^1 and b^2) implemented in ANN are obtained through a training procedure using the Levenberg–Marquardt (LM) algorithm. Different from the approach proposed by Marzano et al. (2004) where only ground radar data from different heights are used as the training dataset, both the reflectivities from RCHL and TRMM PR are used in the training in this study. Before being applied in the training process, the reflectivity fields from RCHL and TRMM PR were processed with the following steps:

1) Applying a quality-control process on the TRMM PR data. The level II algorithm of the PR profile

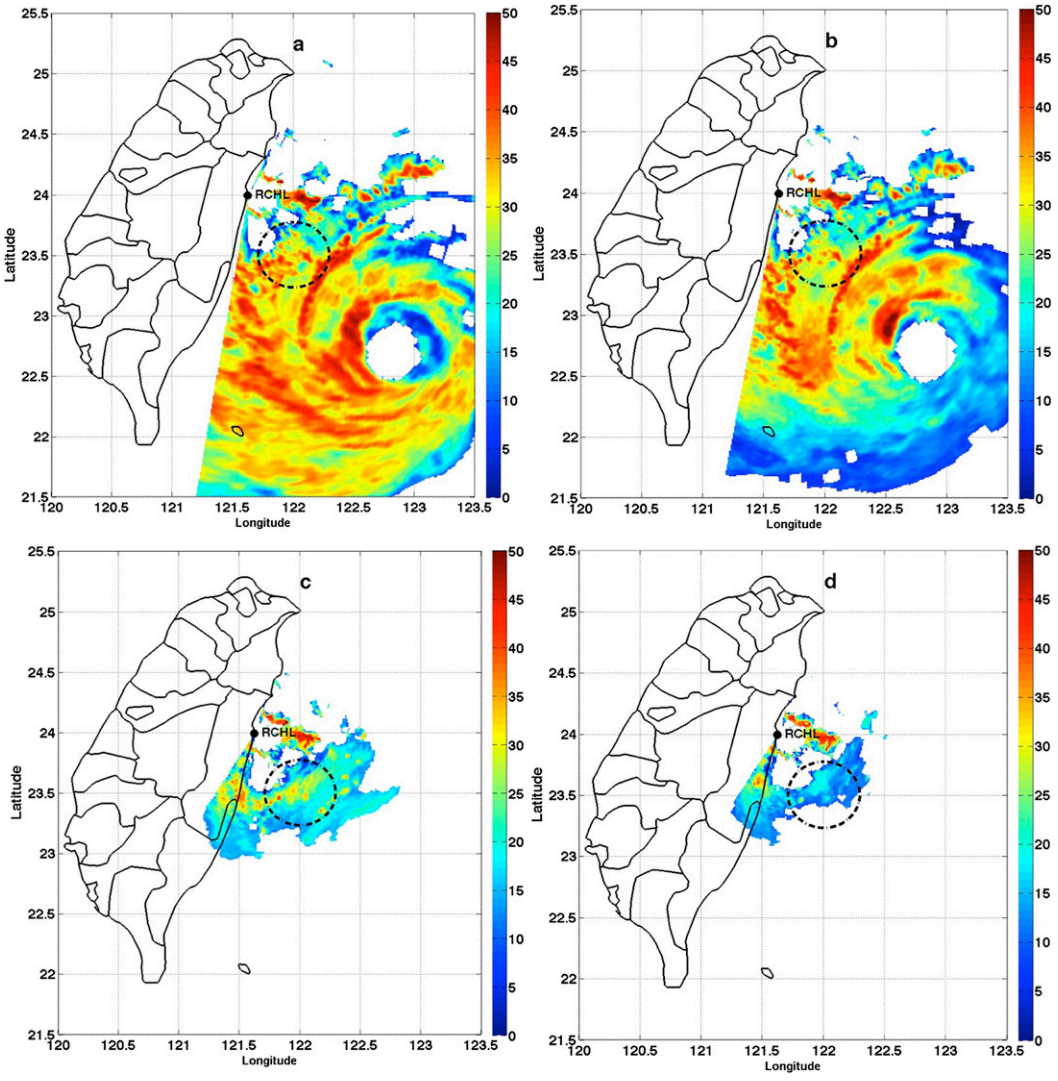

FIG. 4. The reflectivity fields observed by RCHL at 0945 UTC 23 Aug 2012. The mean reflectivities within the black circle at (a) 0.5°, (b) 1.4°, (c) 4.3°, and (d) 6.0° are 29, 27, 19, and 13 dBZ, respectively.

algorithm (2A25) is first applied on the TRMM PR data, and the reflectivity data are corrected from attenuation and ground-clutter filtering. To further minimize the possible effects from the remaining ground clutter, the first three gates (750 m) of the filtered TRMM PR reflectivity are eliminated. The first valid data used in the ANN training are the fourth gate.

2) Converting the RCHL reflectivity field from polar into Cartesian coordinates with the horizontal resolution of 1 km.
3) Converting the horizontal resolution of the RCHL from 1 to 4.3 km through a simple average method. Therefore, the horizontal resolution of RCHL and TRMM PR are matched to each other.
4) Grouping the vertical reflectivities of RCHL and TRMM PR from the same locations (latitude and longitude) as training pairs.
5) Separating all the available training pairs into stratiform and convective types. Since the VPRs from different precipitations could be significantly distinct, using separate ANNs trained from stratiform and convective precipitation types could potentially enhance the VPR correction results.

The approaches developed by Zhang et al. (2008) and Xu et al. (2008) were used in the precipitation type segregation. In the approach proposed by Zhang et al. (2008), a radar bin column is identified as convective if a reflectivity at any height in the column is greater than

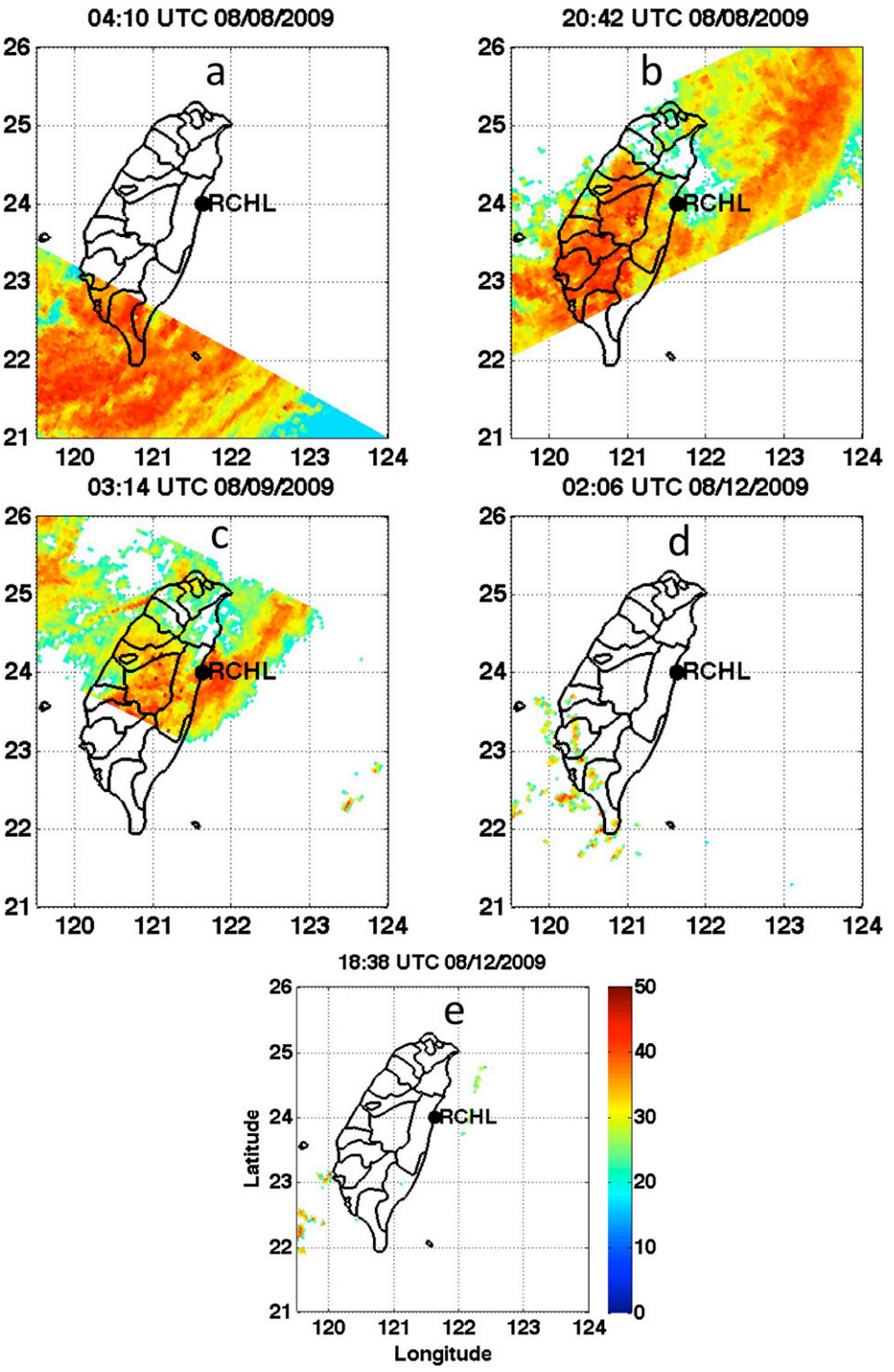

FIG. 5. The reflectivity fields observed by TRMM PR from Typhoon Morakot on 8–12 August 2009.

50 dBZ, or a reflectivity is greater than 30 dBZ at −10°C or above. Otherwise, this radar bin column is identified as stratiform precipitation. A VPR is classified as tropical convective type if the reflectivities monotonically increase or remain constant with the decrease of height (Xu et al. 2008). In this work, the types of convective and tropical convective are merged as convective precipitation, and approximately 70% of the VPRs belong to the convective type for the precipitation events used in the validation. Therefore, two ANNs are obtained for

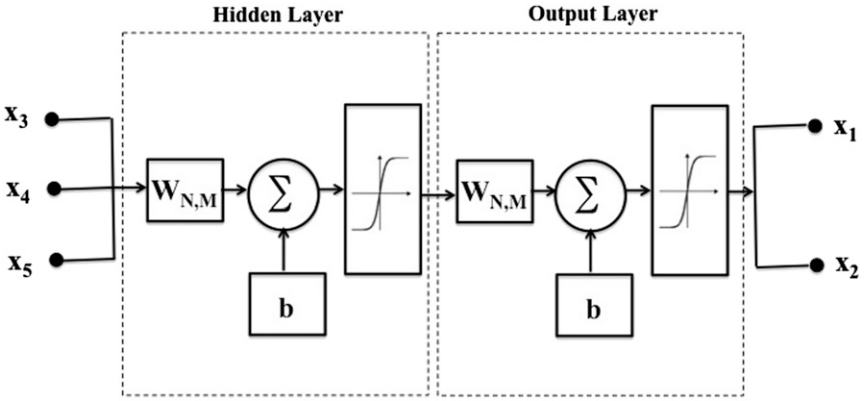

FIG. 6. Flowchart of the developed two layers of ANN for the VPR retrieval, where X_3–X_5 are the radar reflectivities from three higher tilts and X_1 and X_2 are the reconstructed radar reflectivities from the lowest two tilts. The weight matrix $\mathbf{W}_{N,M}$ and the adjusting factor b are trained using the data from TRMM PR and RCHL.

stratiform and convective precipitations, respectively. It should be noted that the radar beam would broaden at far range, which will cause the smoothing effect on the VPR. Although no model-based approach (e.g., Zhang and Qi 2010) was applied to correct the smoothing effect in the VPR derivation, the smoothing effect was considered through limiting the maximum range (80 km) of the ANN approach. Given this relative close range, the impact on the ANN VPR correction is not significant (Marzano et al. 2004).

Examples of training data are demonstrated in Fig. 7, where VPRs from stratiform and convective precipitations are shown in Figs. 7a and 7b, respectively. Reflectivities from RCHL at h_3–h_5 (black lines) and from TRMM PR (gray lines) from the same location are utilized as one pair of the training data. The severe blockage causes the missing radar reflectivities (x_1 and x_2) at the two lowest heights (e.g., h_1 and h_2) for a given azimuth and range. Reflectivities (x_3–x_5) from three higher heights (e.g., h_3–h_5) at the same azimuth and range are used as the inputs to the ANN. The output of the ANN is the normalized reflectivity x_1 (x_2) at height h_1 (h_2). It should be noted that values of x_3–x_5 are normalized to the reflectivity at a reference height (5 km MSL), and the reflectivity at 5 km could be obtained through linear interpolation with x_3–x_5. Given the observed higher-tilt reflectivities x_3–x_5 (at h_3–h_5), the initial guesses of x_1 (at h_1) and x_2 (at h_2) are calculated using initial weighting matrices and adjusting factors. The differences ε between x_1 (x_2) and the TRMM PR reflectivities at h_1 (h_2) are then calculated. The initial weighting matrices and the adjusting factors are then modified in a way that can decrease ε. The training procedure is considered complete when ε reaches a

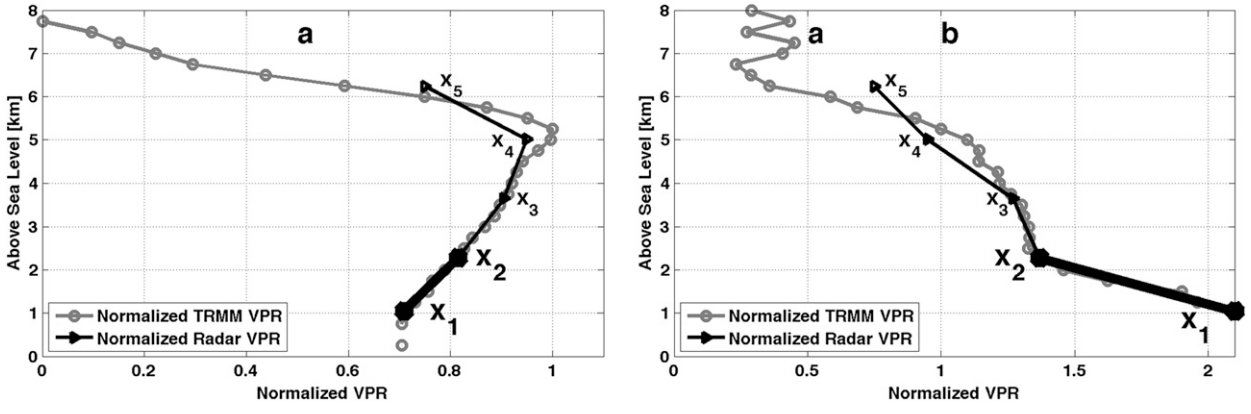

FIG. 7. The normalized VPR observed by RCHL (black lines) and TRMM PR (gray lines), where X_3–X_5 are the RCHL observations from three higher continued elevation angles and X_1 and X_2 are the retrieved reflectivities from two lowest elevation angles. The vertical reflectivity observed from (a) stratiform and (b) convective precipitations are shown.

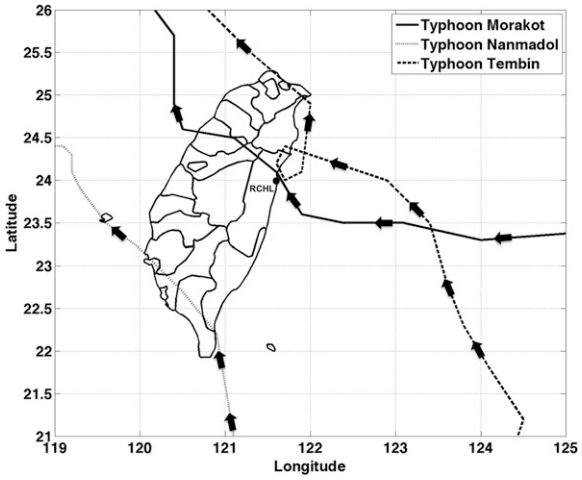

FIG. 8. Typhoon tracks of Morakot (2009), Nanmadol (2011), and Tembin (2012).

minimum value. It should be noted that the maximum height of RCHL and TRMM PR data is 8 km MSL as shown in Fig. 7.

4. Performance evaluation

The new ANN-based VPR correction approach was evaluated using three 24-h typhoon events of Morakot (0000–2400 UTC 8 August 2009), Nanmadol (0000–2400 UTC 28 August 2011), and Tembin (0000–2400 UTC 22 August 2012). During these three typhoon events, TRMM PR passed over the Taiwan region at 2042 UTC 8 August 2009 (Morakot), 0751 UTC 28 August 2011 (Nanmadol), and 0942 UTC 23 August 2012 (Tembin). Tracks of the three typhoons are presented in Fig. 8. All three typhoons moved from the east to the west side of Taiwan, except that the centers of Morakot and Tembin hit northern Taiwan while the center of Nanmadol hit southern Taiwan. Only typhoon events are utilized in the performance evaluation because of two major reasons. The first is that a typhoon is one of the worst threats to the Taiwan region. On average, 3.3 typhoons hit Taiwan each year, causing damages exceeding $520 000 000 with extreme heavy rainfalls and strong winds (Lai and Wu 2010). Obtaining accurate QPEs for flood monitoring and prediction, landslide forecasts, and water resource management during typhoon events is the most important mission of the Central Weather Bureau. The second reason is that it was shown that the variation in the VPR from typhoon (tropical) precipitation is significant (Xu et al. 2008), and the correction on the reflectivity field from typhoon precipitation is necessary to achieve accurate QPE. It is a good option to start this work with the typhoon precipitation. Although a total of 27 typhoon events impacted the Taiwan region during 2001–12, both the radar and TRMM PR data are available only from these three typhoon events from the Taiwan region. For the other 24 events, the TRMM PR did not scan the Taiwan region (or there are no overlaps between scans from RCHL and TRMM PR) during the time period of the typhoon, and therefore they were not used in the current work. One assumption of the neural network approach is the representativeness of the limited training data, which could be used to catch the signatures of the testing data. We assume that within the relatively short period, such as 24 h, the variations in the vertical structure of reflectivity are not significant. Therefore, the two ANNs (stratiform and convective), trained for each typhoon event using the available one volume data, could be used to correct radar reflectivity during the 24 h period.

Four experiments (EXP I–IV; shown in Table 2) were carried out to evaluate the new VPR correction approach. In EXP I, the radar-based rain rate is directly estimated using the higher-tilt reflectivity when the lower-tilt data are blocked by the CMR. In EXP II, the higher-tilt reflectivity is corrected using the normalized VPR derived from RCHL (denoted as VPR-RCHL) based on the observations to the east of RCHL. In EXP III and IV, the higher-tilt reflectivity is corrected using the VPR derived from the TRMM PR data. EXP III uses the mean VPR-TRMM, and EXP IV uses the VPR calculated from the new developed ANN approach, respectively. In all VPR approaches (EXP II–IV), the observed higher-tilt reflectivity is corrected as

$$Z^{\mathrm{Cor}} = Z^{\mathrm{Obs}} \frac{\mathrm{VPR}(H_2)}{\mathrm{VPR}(H_1)}, \tag{3}$$

where Z^{Obs} is the observed reflectivity at height H_1; Z^{Cor} is the corrected reflectivity; and VPR(H_2) and VPR(H_1) are the normalized VPRs at heights H_2 (the height from higher tilt, that is, the height of Z^{Obs}) and H_1 (the terrain height), respectively. Two reflectivity–rain rate (Z–R) relationships are utilized in the rain-rate estimation, one for convective ($Z = 88R^{1.64}$) and one for stratiform ($Z = 131R^{1.72}$) precipitation. These two relationships were derived using the drop size distribution (DSD) data collected by four impact-type Joss–Waldvogel disdrometers (JWD; as indicated in Fig. 1). The measurement range of JWD is between 0.359 and 5.373 mm with 20 bins, and temporal resolution is 1 min. A total of 7920 min of DSD data were used in the Z–R relationships derivation.

In the evaluation, the rain rate (updated every 5 min) was first estimated with the Z–R relationship according to the precipitation classification result, and then the

TABLE 2. Comparison results of MR, RMSE, and CC obtained in EXP I–IV. For EXP II–IV, the improvement percentages according to EXP I are also included.

	EXP I no VPR correction	EXP II VPR-RCHL correction	EXP III VPR-TRMM (mean) correction	EXP IV VPR-TRMM (ANN) correction
Typhoon Morakot				
MR	0.60	0.63 (3%)	0.74 (14%)	1.06 (34%)
RMSE (mm)	61	58 (5%)	47 (23%)	43 (30%)
CC	−0.32	−0.30 (0%)	0.13 (13%)	0.30 (30%)
Typhoon Nanmadol				
MR	0.33	0.39 (6%)	0.48 (15%)	0.60 (27%)
RMSE (mm)	187	175 (6%)	155 (17%)	116 (38%)
CC	0.26	0.29 (3%)	0.37 (11%)	0.63 (37%)
Typhoon Tembin				
MR	0.58	0.67 (9%)	1.12 (30%)	1.03 (39%)
RMSE (mm)	64	60 (6%)	56 (12%)	50 (22%)
CC	0.21	0.32 (11%)	0.63 (42%)	0.67 (46%)
Total				
MR	0.43	0.48 (5%)	0.59 (16%)	0.78 (35%)
RMSE (mm)	123	116 (5%)	107 (13%)	84 (32%)
CC	0.33	0.37 (4%)	0.45 (11%)	0.60 (27%)

24-h precipitation accumulation was calculated. QPE results from these four experiments were compared with surface rain gauge measurements. The gauge network (shown in Fig. 1) consists of a total of 494 surface stations, and automatic rainfall and meteorological telemetry system stations. The original goal of the gauge network is to provide effective real-time rainfall and hourly meteorological observation data (Chen et al. 1999). A detailed description of the gauge network can be found in the publication produced by Central Weather Bureau (Central Weather Bureau 1995). Among these 494 gauges, 43 of them (marked as red dots) were used in this work for the performance evaluation. Three scores were used to assess the performance of each experiment: 1) the mean ratio [MR; where MR = $(R_p)/(G_p)$]; 2) the root-mean-square error {RMSE; where RMSE = $[(R_p - G_p)^2]^{1/2}$}; and 3) the correlation coefficient (CC; where CC = $\{[R_p - (R_p)][G_p - (G_p)]\}/\sigma_R\sigma_G$), where R_p (G_p) is the 24-h radar (gauge) accumulated rainfall for each pair p and σ_R (σ_G) is the standard deviation of all the radar (gauge) pairs.

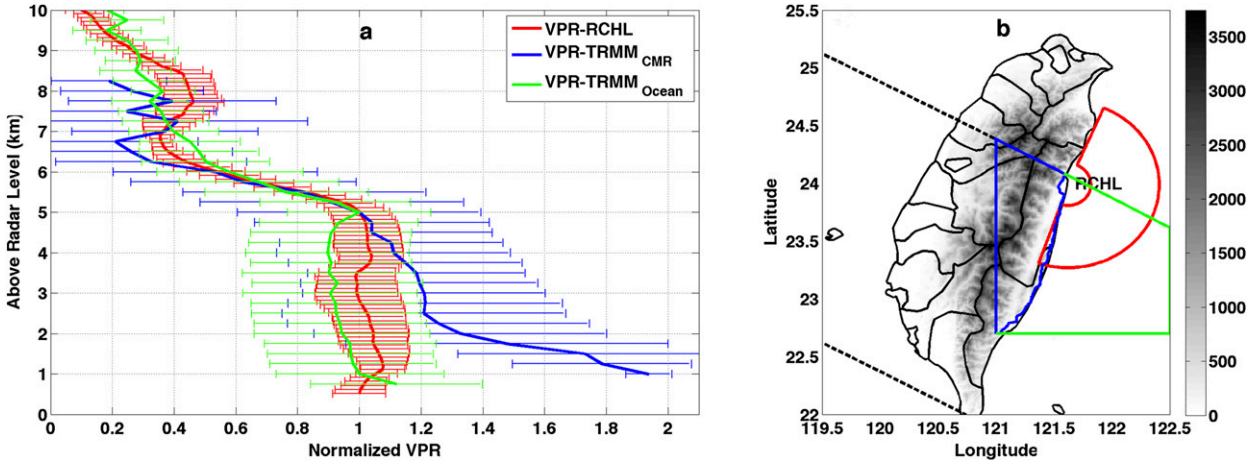

FIG. 9. (a) The mean VPR sampled by RCHL (VPR-RCHL) and TRMM PR using the data from the CMR (VPR-TRMM$_{CMR}$) or ocean (VPR-TRMM$_{Ocean}$) regions are plotted using red, blue, and green thick lines, respectively. The std dev at each height is included as a thin bar. The mean VPR-RCHL was derived using a volume scan of reflectivity at 0758 UTC 28 Aug 2011, and the mean VPR-TRMM was derived using the TRMM PR data at 0751 UTC 28 Aug 2011. (b) A map showing the radar data used in the VPR-RCHL derivation (red lines) and the TRMM PR data used in the VPR-TRMM$_{CMR}$ and VPR-TRMM$_{Ocean}$ derivation (blue and green lines, respectively). The TRMM PR swath is also shown (black dashed lines).

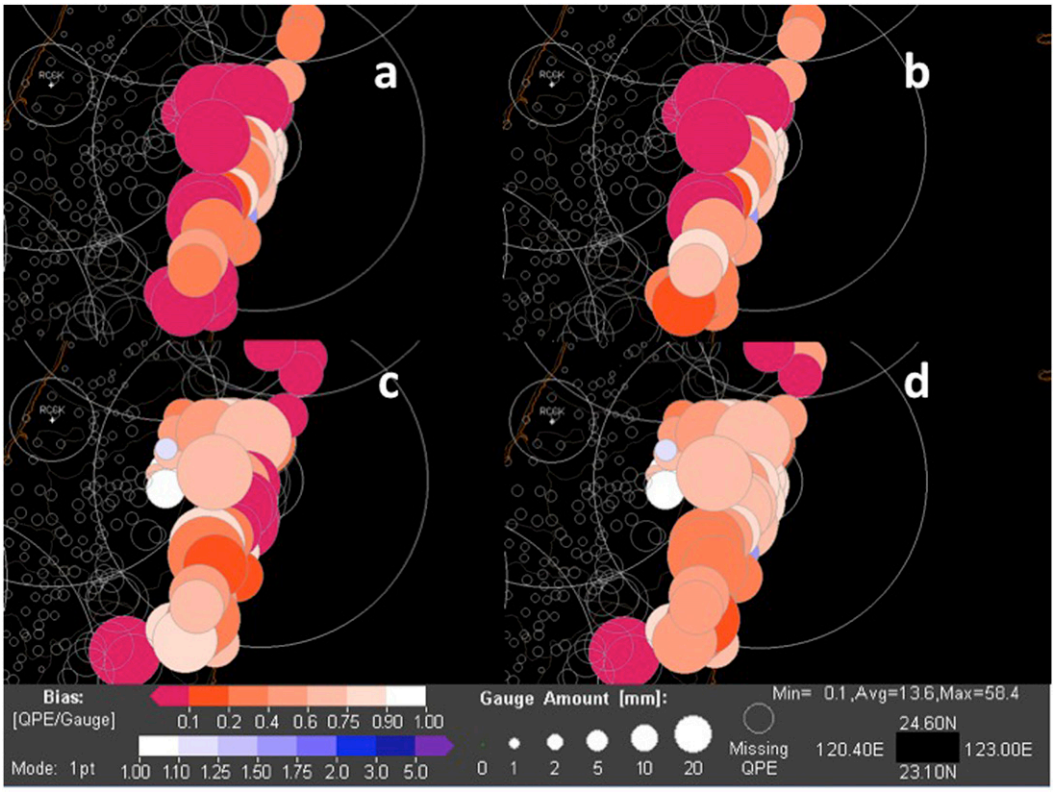

FIG. 10. Spatial distribution of the radar QPE vs gauge observations (a) without VPR correction, (b) with VPR correction where the VPRs are derived using mean VPR-RCHL, (c) using mean VPR-TRMM, and (d) using VPR-TRMM reconstructed from ANN. The 24-h accumulated precipitation from Typhoon Nanmadol (0000–2400 UTC 28 Aug 2011) is used in this experiment. The size of the circles represents gauge-observed accumulated amount, and the color of the circles indicates the bias (QPE/Gauge).

a. Case I

Typhoon Nanmadol is of primary interest because of its significant precipitation on the east coast and the obvious vertical structure in the reflectivity field. Nanmadol was formed on 21 August 2011 and made its landfall over the Taiwan region on 28 August. Along the east coast, the maximum 24-h accumulation measured by the gauges is approximately 374 mm. The TRMM PR passed over Taiwan at 0751 UTC 28 August 2011 and provided data for the neural network training. There are a total of 204 pairs of RCHL and TRMM PR vertical reflectivity columns (with 4.3-km resolution) used in the ANN training.

To demonstrate the VPR correction performances, a comparison of the normalized VPRs derived from RCHL (VPR-RCHL) and TRMM PR (VPR-TRMM) is depicted in Fig. 9a. In this example, the means and standard deviations of VPR-RCHL derived using the approach proposed by Zhang et al. (2008) are presented in Fig. 9a with red lines. In this approach, a volume scan of reflectivity data (at 0758 UTC 28 August 2011) first goes through a neural network–based quality-control procedure (Lakshmanan et al. 2007) to remove ground clutter. The quality-controlled reflectivity data from all tilts are interpolated onto evenly spaced vertical heights that are 200 m apart according to the central height of the reflectivity bins. Only those data within the annular region (red in Fig. 9b) of the 20–80-km range, which are free of terrain blockages, are selected in the VPR derivation. As shown in Fig. 9a, the mean reflectivities at each level are normalized with respect to the values at a reference height (5 km MSL in this work). Two mean VPRs were derived using TRMM PR data at 0751 UTC 28 August 2011 from different regions: the CMR denoted as VPR-TRMM$_{CMR}$ (thick blue line) and the ocean denoted as VPR-TRMM$_{Ocean}$ (thick green line). The data used in VPR-TRMM$_{CMR}$ (VPR-TRMM$_{Ocean}$) derivation are from the blue (green) region shown in Fig. 9b. The means and standard deviations calculated using all of the available TRMM PR data within each 250-m height layer are presented with thick and thin lines, respectively. Because the TRMM PR is operated at Ku band with a frequency of 13.8 GHz (2.17-cm

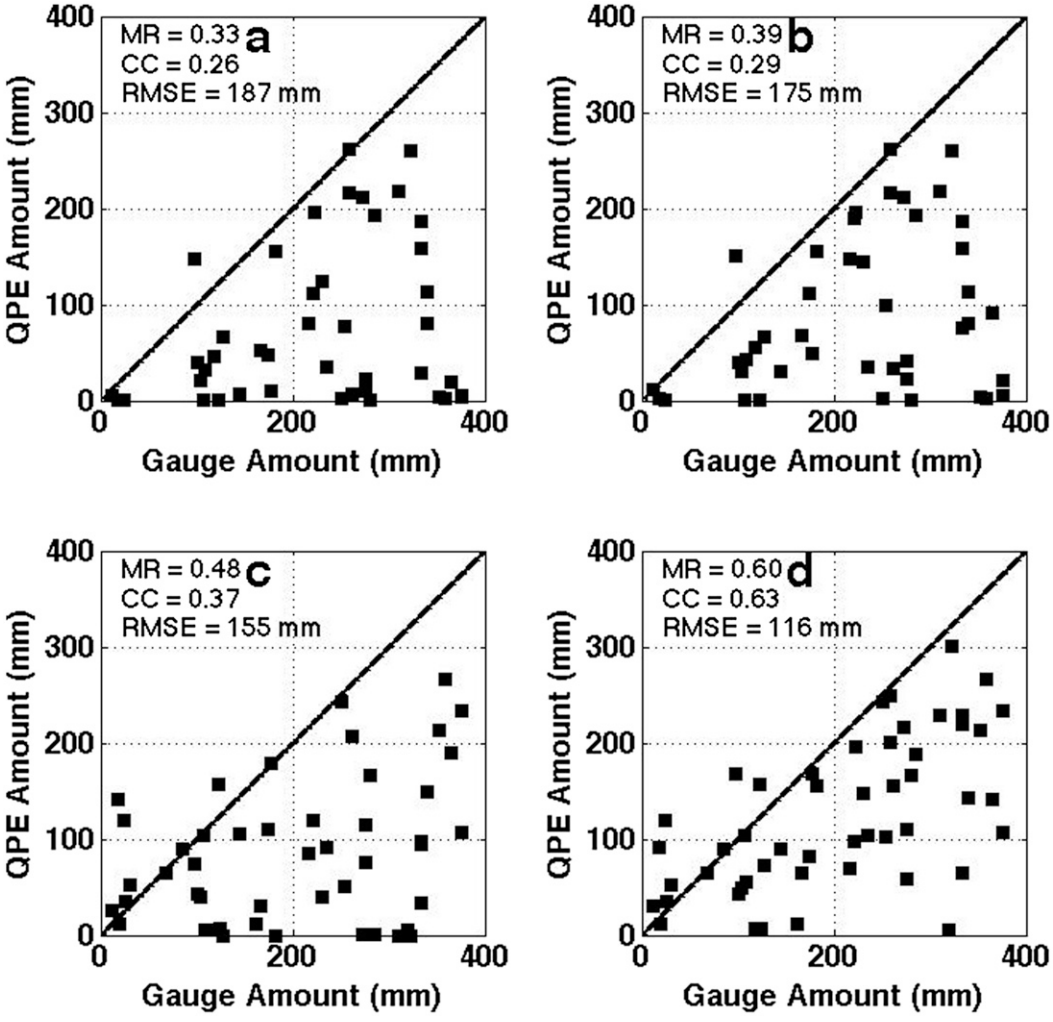

FIG. 11. Scatterplots of the radar QPE vs gauge observations for Typhoon Nanmadol (0000–2400 UTC 28 Aug 2011). The reflectivity fields used in the rain-rate estimation are (a) without VPR correction, (b) with VPR correction where the VPRs are derived using mean VPR-RCHL, (c) using mean VPR-TRMM, and (d) using VPR-TRMM reconstructed from ANN. The evaluation results in terms of mean bias, CC, and RMSE are also included.

wavelength), the attenuation correction is necessary for the TRMM PR observations when they are used in the VPR derivation. In this example, VPR-RCHL, VPR-TRMM$_{CMR}$, and VPR-TRMM$_{Ocean}$ showed similar trends above 5 km, especially between 5 and 7 km (Fig. 9a). The mean reflectivities from these three VPRs decrease with increasing heights. However, apparent disparities can be observed below 5 km MSL, where VPR-TRMM$_{CMR}$ shows larger values than VPR-RCHL at any given height. The differences between VPR-RCHL and VPR-TRMM$_{Ocean}$ are relatively smaller. For example, the normalized mean VPR-TRMM$_{CMR}$ increases from 1.0 (5 km) to 1.78 (1 km), but the normalized mean VPR-RCHL increases from 1 (5 km) to 1.05 (1 km). The difference between these two normalized VPRs is more than 50%, which will result in significantly different correction results when they are applied in the VPR correction. On the other hand, the normalized mean VPR-TRMM$_{Ocean}$ almost remains the same from 1 to 5 km. The variations of VPR-RCHL and VPR-TRMM$_{Ocean}$ between 1 and 5 km are very similar. Two factors could potentially cause the differences between VPR-RCHL and VPR-TRMM$_{CMR}$. First, the radar data used in the VPR-RCHL derivation were mainly from the ocean area (red in Fig. 9b) but VPR-TRMM$_{CMR}$ data were from the land (blue in Fig. 9b). Different atmospheric environments (over land and ocean) could cause different microphysical processes at the lower altitudes and result in different VPRs near the surface. Second, most of the data used in the VPR-TRMM$_{CMR}$

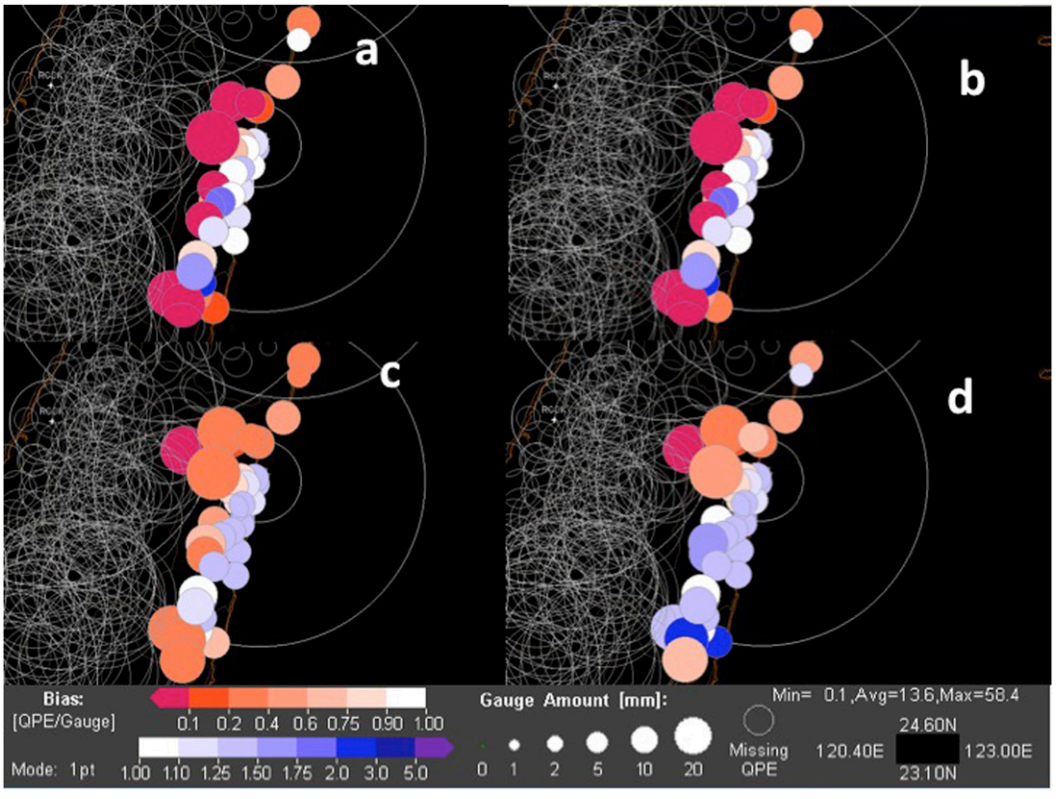

FIG. 12. Spatial distribution of the radar QPE vs gauge observations (a) without VPR correction, (b) with VPR correction where the VPRs are derived using mean VPR-RCHL, (c) using mean VPR-TRMM, and (d) using VPR-TRMM reconstructed from ANN. The 24-h accumulated precipitation from Typhoon Morakot (0000–2400 UTC 8 Aug 2009) is used in this experiment. The size of the circles represents gauge-observed accumulated amount, and the color of the circles indicates the bias (QPE/Gauge).

derivation were from the mountainous region. The large increase of reflectivity with decreasing height in VPR-$TRMM_{CMR}$ is most likely an indication of significant orographic enhancement of precipitation. A similar phenomenon was also observed in the mountain regions of the western United States (Zhang et al. 2012). Moreover, the lower sensitivity of TRMM PR to low reflectivity may also cause the large VPR. Since both VPR-RCHL and VPR-$TRMM_{Ocean}$ are obtained from the data sampled from the ocean region, differences between VPR-RCHL and VPR-$TRMM_{Ocean}$ are smaller than differences between VPR-RCHL and VPR-$TRMM_{CMR}$ at each height layer.

Figure 10 shows the bias ratios of the four radar QPEs versus gauge observations on the 24-h scale. The bubble size indicates the amount of the 24-h gauge observation, and the bubble color indicates the ratio between the radar QPE and the gauge observation. Warm (from orange to red), cool (from blue to purple), and white colors represent the radar QPE overestimation, underestimation, and matching with gauge, respectively. Corresponding scatterplots are also presented in Fig. 11, where the scores of MR, CC, and RMSE are included as a reference.

In EXP I (Fig. 10a), significant underestimation could be observed along the east coast of Taiwan. The maximum difference between the gauge measurement and QPE is 356 mm, and the means of gauge measurement and QPE are 225 and 63 mm. The MR, RMSE, and CC of EXP I in this case are 0.33, 187 mm, and 0.26, respectively. Because of the severe beam blockage, reflectivity data from a tilt under 2.4° are not available, as shown in Fig. 3, and only data from 2.4° and above could be applied in rain-rate estimation. The nonuniform vertical structure in the reflectivity field, which causes the low correlation between the higher-tilt reflectivity and the ground precipitation intensity, is the major cause of the underestimation. Relatively low reflectivity data from a higher tilt could be found in the VPR example in Fig. 9, and the underestimation results when the low reflectivity is applied in the rain-rate estimation. In EXP II, although the higher-tilt reflectivity is

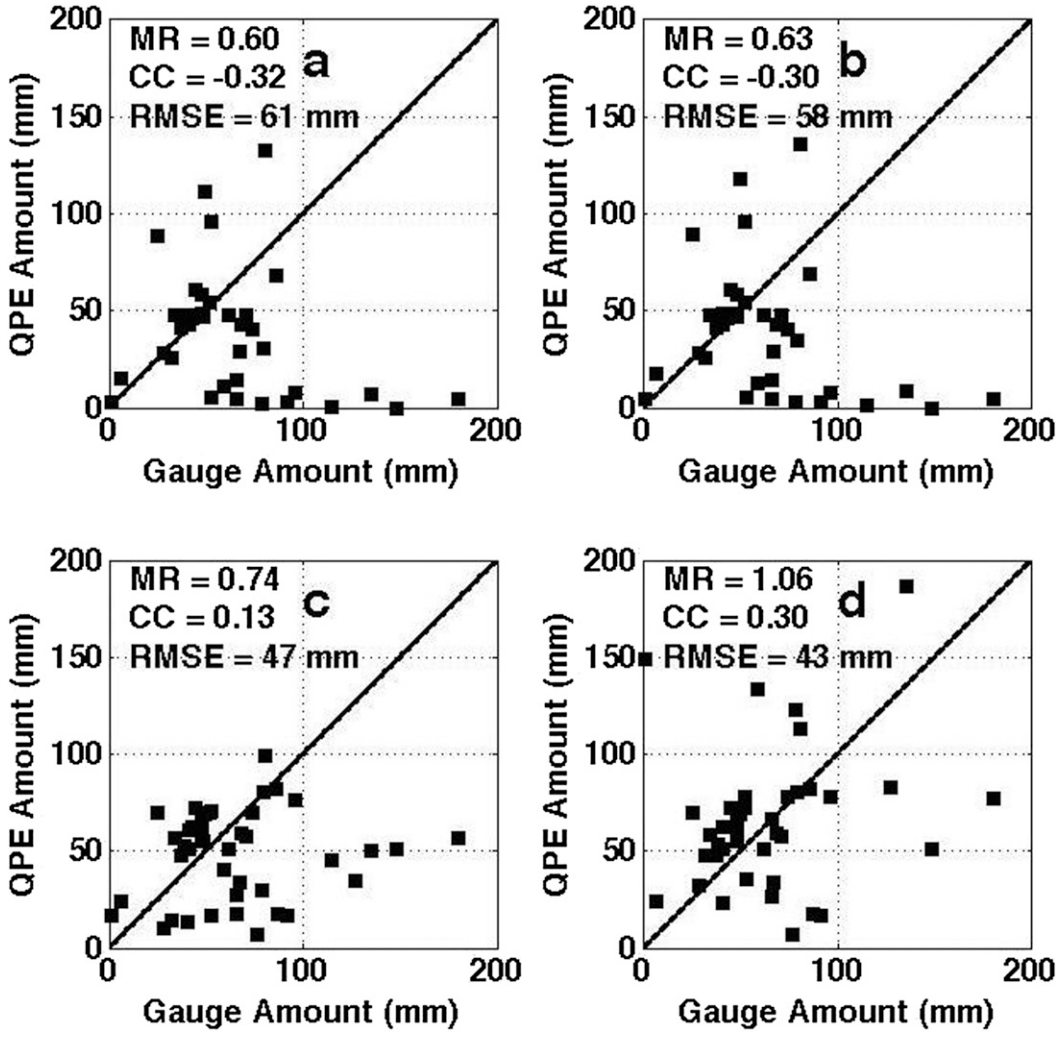

FIG. 13. Scatterplots of the radar QPE vs gauge observations for Typhoon Morakot (0000–2400 UTC 8 Aug 2009). The reflectivity fields used in the rain-rate estimation are (a) without VPR correction, (b) with VPR correction where the VPRs are derived using mean VPR-RCHL, (c) using mean VPR-TRMM, and (d) using VPR-TRMM reconstructed from ANN. The evaluation results in terms of mean bias, CC, and RMSE are also included.

corrected using the VPR derived from radar observations to the east of RCHL, the underestimation had limited improvement over EXP I with the MR, RMSE, and CC of 0.39, 175 mm, and 0.29, respectively. As demonstrated in Fig. 9, the normalized VPR from a lower altitude (e.g., 1 km MSL) is approximately the same as the value from a higher altitude (e.g., 4 km MSL). This is because the VPR-RCHL derived from the ocean area cannot catch the vertical structure of the precipitation over the steep mountain area west of RCHL. On the other hand, apparent improvements could be obtained after the higher-tilt reflectivity is corrected using the VPR derived using the mean VPR-TRMM as shown in Fig. 10c. The MR and CC are increased to 0.48 and 0.37, and the RMSE drops to 155 mm. The improvements come from the VPR-TRMM, which better captured the vertical structure of reflectivity in the mountainous region west of RCHL during typhoons (Fig. 9a), especially the orographic precipitation enhancements near the surface. However, because of the large variance observed from the VPR-TRMM as shown in Fig. 9a, biased correction results if the mean VPR-TRMM is directly used in the VPR correction. On the other hand, the trained ANN can build the correlation between the "local" observed TRMM and radar VPRs, and the uncertainty from the mean VPR-TRMM is therefore decreased. Using the trained ANN, the most likely low-tilt radar reflectivity can be estimated given the higher-tilt observations. The obtained MR, RMSE, and CC are 0.60, 116 mm, and

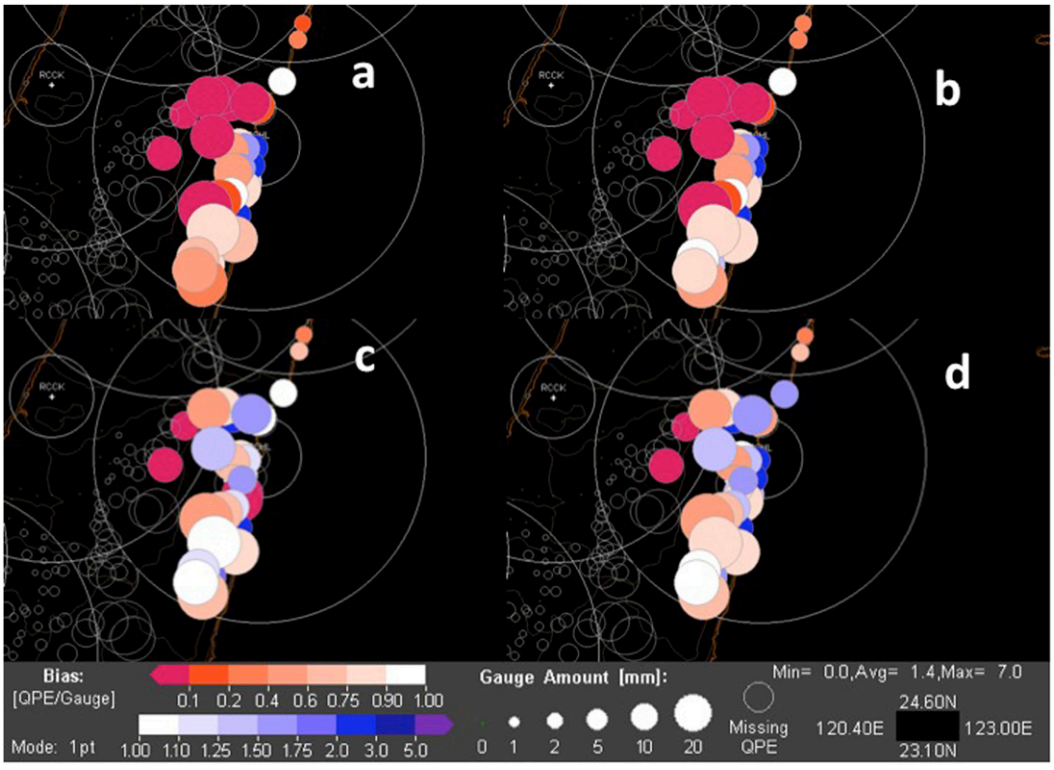

FIG. 14. Spatial distribution of the radar QPE vs gauge observations (a) without VPR correction, (b) with VPR correction where the VPRs are derived using mean VPR-RCHL, (c) using mean VPR-TRMM, and (d) using VPR-TRMM reconstructed from ANN. The 24-h accumulated precipitation from Typhoon Tembin (0000–2400 UTC 23 Aug 2012) is used in this experiment. The size of the circles represents gauge-observed accumulated amount, and the color of the circles indicates the bias (QPE/Gauge).

0.63, respectively. Compared to EXP I, EXPs II–IV improve MR (6%, 15%, and 27%), RMSE (6%, 17%, and 38%), and CC (3%, 11%, and 37%).

b. *Cases II and III*

The deadliest typhoon in the recorded history of Taiwan, Typhoon Morakot formed on 2 August 2009 and dissipated on 12 August 2009. Morakot landed on Taiwan at midnight (local time) on 8 August and brought a maximum accumulated precipitation of 2600 mm during 4 days (Wang et al. 2013). In EXP I (Fig. 12a), underestimation, indicated by red bubbles, could be observed along the east coast of Taiwan. The maximum difference between the gauge measurement and QPE is 148.5 mm, and the means of gauge measurement and QPE are 62.39 and 38.57 mm, respectively. The MR, RMSE, and CC of EXP I in this case are 0.60, 61 mm, and −0.32, respectively. A negative correlation coefficient indicated that the radar-based QPE was uncorrelated to the gauge observations. Similar to case I, although the higher-tilt reflectivity is corrected in EXP II using the VPR derived from radar observations to the east of RCHL, the underestimation had limited improvement over EXP I with the MR, RMSE, and CC of 0.63, 58 mm, and −0.30, respectively. The underestimation is mitigated using the new ANN approach as shown in Fig. 12d, where MR, RMSE, and CC are improved to 1.06, 43 mm, and 0.30, respectively. The percentages of the enhancement on each score are also included in Table 2. The better vertical reflectivity structure captured by TRMM PR and the ANN approach are the two key factors causing the apparent improvements. The scatterplots of the comparison between radar QPE and gauge observations are presented in Fig. 13. There are a total of 133 pairs of RCHL and TRMM PR vertical reflectivity columns are used in the ANN training.

The performance of EXP I–IV was also evaluated using a 24-h precipitation event during Typhoon Tembin (0000–2400 UTC 23 August 2012) as shown in Figs. 14 and 15.

Comparison results from these four EXPs are also included in Table 2. There are total of 214 pairs of RCHL and TRMM PR vertical reflectivity columns are used in the ANN training.

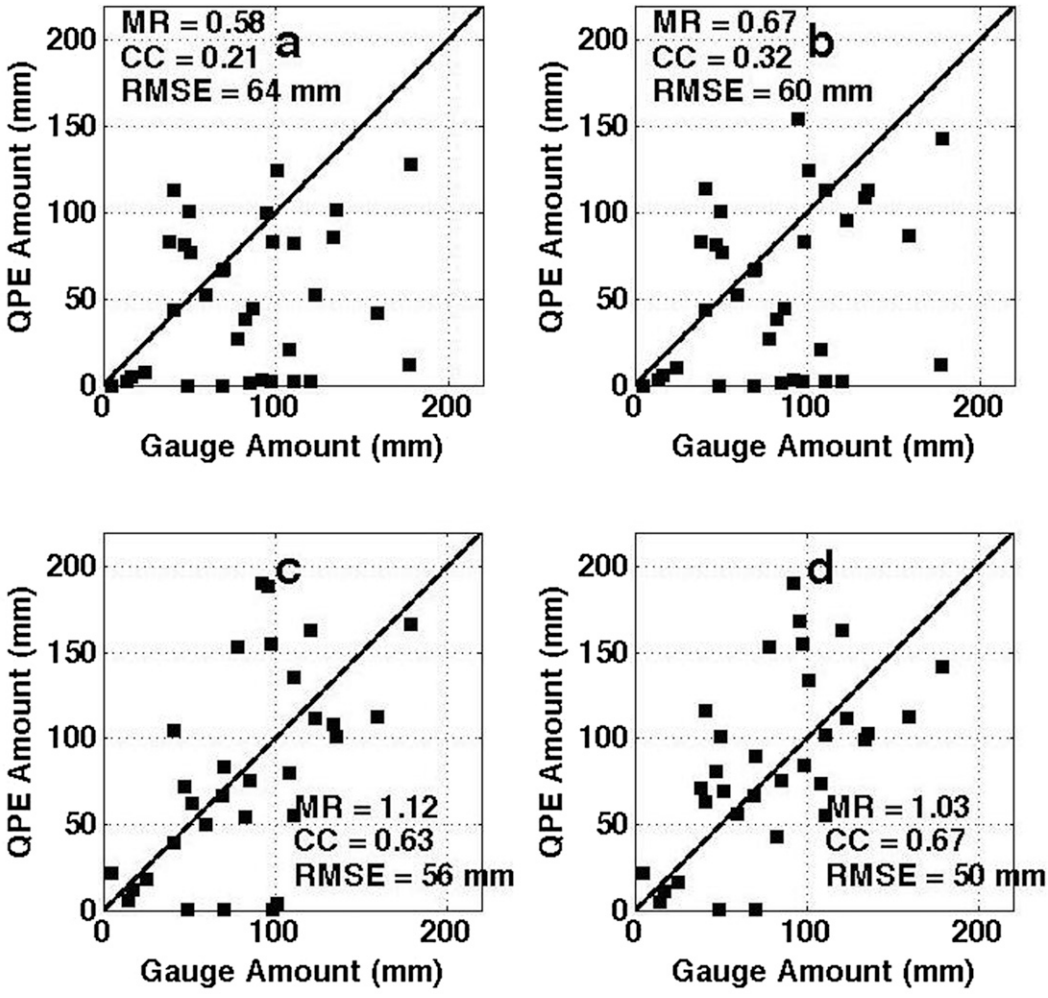

FIG. 15. Scatterplots of the radar QPE vs gauge observations for Typhoon Tembin (0000–2400 UTC 23 Aug 2012). The reflectivity fields used in the rain-rate estimation are (a) without VPR correction, (b) with VPR correction where the VPRs are derived using mean VPR-RCHL, (c) using mean VPR-TRMM, and (d) using VPR-TRMM reconstructed from ANN. The evaluation results in terms of mean bias, CC, and RMSE are also included.

5. Summary and conclusions

In the ground radar–based quantitative precipitation estimation, the higher-tilt reflectivity data are generally used in the rain-rate estimation when the lower-tilt data are blocked from complex terrain. However, biases could be introduced into the QPE because of vertical variations in the reflectivity field. To obtain accurate radar QPE when severe blockages are present, a vertical profile of reflectivity correction using TRMM PR data with an artificial neural network (ANN) has been developed. The ANN is trained using the reflectivity fields observed by an S-band Doppler weather radar located on the east coast of Taiwan (RCHL) and by the TRMM PR. During the training process, the vertical structure of reflectivity observed by TRMM PR was treated as the ''true'' VPR, and the training of ANN was aimed at minimizing the difference between the retrieved radar reflectivity and the corresponding TRMM PR observation at a reference level near the ground. The proposed approach was evaluated using three 24-h typhoon events. The higher-tilt radar data were corrected using the trained ANN before being used in the rain-rate estimation, and the radar-based QPE was compared with gauge observations. Compared to the VPR correction approach based on the VPR-RCHL, the new reflectivity correction approach can better retrieve reflectivities using the observations at the higher unblocked tilts. Two factors are the major reasons for the improvement: 1) the VPR-TRMM can better capture the orographic

precipitation enhancements and 2) the proposed ANN can better generate the relation between the higher-tilt observation and lower-tilt reflectivity.

While the current approach is not ready for real-time QPE applications, it provides a way of integrating a spaceborne radar and ground radar data for the purpose of enhanced QPE. There are some limitations with the current approach that warrant further study. First, near-surface observations from TRMM PR may not be reliable and residual clutter may impact the correction results. Second, correlations between radar measurements and surface precipitation decrease with increasing height of the radar data and the VPR correction range cannot be far. Third, the relatively small training dataset potentially limited the usefulness of the current scheme. The proposed ANN approach might be further enhanced had more data been included in the training process. Fourth, rainfall intensities over complex orography depend on the direction of flow with respect to the mountain slopes. Because of the limited dataset, the flow regime was not taken into account in the current work. With the recent launch of the Global Precipitation Measurement satellites, the current scheme can be enhanced with higher spatial– and higher temporal–resolution spaceborne radar data and potentially further improve ground radar QPEs for hydrological predictions in areas with poor radar coverage.

Acknowledgments. This research is supported by funding from the Central Weather Bureau of Taiwan, Republic of China, and was provided by NOAA/Office of Oceanic and Atmospheric Research under NOAA–University of Oklahoma Cooperative Agreement NA110AR4320072, U.S. Department of Commerce. Authors would like to thank Dr. Lin Tang for providing many helpful comments and that greatly improved the manuscript.

REFERENCES

Andrieu, H., and J. D. Creutin, 1995: Identification of vertical profiles of radar reflectivity for hydrological applications using an inverse method. Part I: Formulation. *J. Appl. Meteor.*, **34**, 225–239, doi:10.1175/1520-0450(1995)034<0225:IOVPOR>2.0.CO;2.

Bankert, R. L., and D. W. Aha, 1996: Improvement to a neural network cloud classifier. *J. Appl. Meteor.*, **35**, 2036–2039, doi:10.1175/1520-0450(1996)035<2036:ITANNC>2.0.CO;2.

Cao, Q., Y. Hong, J. J. Gourley, Y. Qi, J. Zhang, Y. Wen, and P.-E. Kirstetter, 2013a: Statistical and physical analysis of the vertical structure of precipitation in the mountainous west region of the United States using 11+ years of spaceborne observations from TRMM Precipitation Radar. *J. Appl. Meteor. Climatol.*, **52**, 408–424, doi:10.1175/JAMC-D-12-095.1.

——, ——, Y. Qi, Y. Wen, J. Zhang, J. J. Gourley, and L. Liao, 2013b: Empirical conversion of the vertical profile of reflectivity from Ku-band to S-band frequency. *J. Geophys. Res. Atmos.*, **118**, 1814–1825, doi:10.1002/jgrd.50138.

Central Weather Bureau, 1995: *The Basic Information of Meteorological Observation Statistic* (in Chinese). 4th ed. Central Weather Bureau, 163 pp. [Available from the Central Weather Bureau, 64 Kung-Yun Rd., Taipei, Taiwan.]

Chen, T.-C., M.-C. Yen, J.-C. Hsieh, and R. W. Arritt, 1999: Diurnal and seasonal variations of the rainfall measured by the automatic rainfall and meteorological telemetry system in Taiwan. *Bull. Amer. Meteor. Soc.*, **80**, 2299–2312, doi:10.1175/1520-0477(1999)080<2299:DASVOT>2.0.CO;2.

Daly, C., R. P. Neilson, and D. L. Phillips, 1994: A statistical–topographic model for mapping climatological precipitation over mountainous terrain. *J. Appl. Meteor.*, **33**, 140–158, doi:10.1175/1520-0450(1994)033<0140:ASTMFM>2.0.CO;2.

Fabry, F., and I. Zawadzki, 1995: Long-term radar observations of the melting layer of precipitation and their interpretation. *J. Atmos. Sci.*, **52**, 838–851, doi:10.1175/1520-0469(1995)052<0838:LTROOT>2.0.CO;2.

Germann, U., and J. Joss, 2002: Mesobeta profiles to extrapolate radar precipitation measurements above the Alps to the ground level. *J. Appl. Meteor.*, **41**, 542–557, doi:10.1175/1520-0450(2002)041<0542:MPTERP>2.0.CO;2.

Goudenhoofdt, E., and L. Delobbe, 2009: Evaluation of radar–gauge merging methods for quantitative precipitation estimates. *Hydrol. Earth Syst. Sci.*, **13**, 195–203, doi:10.5194/hess-13-195-2009.

Hall, T., H. E. Brooks, and C. A. Doswell III, 1999: Precipitation forecasting using a neural network. *Wea. Forecasting*, **14**, 338–345, doi:10.1175/1520-0434(1999)014<0338:PFUANN>2.0.CO;2.

Harrold, T. W., and P. G. Kitchingam, 1975: Measurement of surface rainfall using radar when the beam intersects the melting layer. Preprints, *16th Radar Meteorology Conf.*, Houston, TX, Amer. Meteor. Soc., 473–478.

Hsu, K., H. V. Gupta, and S. Sorooshian, 1995: Artificial neural network modeling of the rainfall–runoff process. *Water Resour. Res.*, **31**, 2517–2530, doi:10.1029/95WR01955.

Hung, N. Q., M. S. Babel, S. Weesakul, and N. K. Tripathi, 2009: An artificial neural network model for rainfall forecasting in Bangkok, Thailand. *Hydrol. Earth Syst. Sci.*, **13**, 1413–1425, doi:10.5194/hess-13-1413-2009.

Iguchi, T., T. Kozu, R. Meneghini, J. Awaka, and K. Okamoto, 2000: Rain-profiling algorithm for the TRMM precipitation radar. *J. Appl. Meteor.*, **39**, 2038–2052, doi:10.1175/1520-0450(2001)040<2038:RPAFTT>2.0.CO;2.

——, ——, J. Kwiatkowski, R. Meneghini, J. Awaka, and K. Okamoto, 2009: Uncertainties in the rain profiling algorithm for the TRMM precipitation radar. *J. Meteor. Soc. Japan*, **87A**, 1–30, doi:10.2151/jmsj.87A.1.

Joss, J., and A. Waldvogel, 1970: A method to improve the accuracy of radar measured amounts of precipitation. Preprints, *14th Radar Meteorology Conf.*, Tucson, AZ, Amer. Meteor. Soc., 237–238.

Kirstetter, P., H. Andrieu, G. Delrieu, and B. Boudevillain, 2010: Identification of vertical profiles of reflectivity for correction of volumetric radar data using rainfall classification. *J. Appl. Meteor. Climatol.*, **49**, 2167–2180, doi:10.1175/2010JAMC2369.1.

Kitchen, M., 1997: Towards improved radar estimates of surface precipitation at long range. *Quart. J. Roy. Meteor. Soc.*, **123**, 145–163, doi:10.1002/qj.49712353706.

Kozu, T., and Coauthors, 2001: Development of precipitation radar onboard the Tropical Rainfall Measuring Mission (TRMM)

satellite. *IEEE Trans. Geosci. Remote Sens.*, **39**, 102–116, doi:10.1109/36.898669.

Kummerow, C., and Coauthors, 2000: The status of the Tropical Rainfall Measuring Mission (TRMM) after two years in orbit. *J. Appl. Meteor.*, **39**, 1965–1982, doi:10.1175/1520-0450(2001)040<1965:TSOTTR>2.0.CO;2.

Lai, L.-H., and P.-H. Wu, 2010: Risk analysis of rice losses caused by typhoon for Taiwan. *Contemp. Manage. Res.*, **6**, 141–158.

Lakshmanan, V., A. Frit, T. Smith, K. Hondl, and G. J. Stumpf, 2007: An automated technique to quality control radar reflectivity data. *J. Appl. Meteor.*, **46**, 288–305, doi:10.1175/JAM2460.1.

Luk, K. C., J. E. Ball, and A. Sharma, 2001: An application of artificial neural networks for rainfall forecasting. *Math. Comput. Modell.*, **33**, 683–693, doi:10.1016/S0895-7177(00)00272-7.

Marzano, F. S., G. Vulpiani, and E. Picciotti, 2004: Rain field and reflectivity vertical profile reconstruction from C-band radar volumetric data. *IEEE Trans. Geosci. Remote Sens.*, **42**, 1033–1046, doi:10.1109/TGRS.2003.820313.

Marzban, C., and G. J. Stumpf, 1998: A neural network for damaging wind prediction. *Wea. Forecasting*, **13**, 151–163, doi:10.1175/1520-0434(1998)013<0151:ANNFDW>2.0.CO;2.

Meneghini, R., T. Iguchi, T. Kozu, L. Liao, K. Okamoto, J. A. Jones, and J. Kwiatkowski, 2000: Use of the surface reference technique for path attenuation estimates from the TRMM precipitation radar. *J. Appl. Meteor.*, **39**, 2053–2070, doi:10.1175/1520-0450(2001)040<2053:UOTSRT>2.0.CO;2.

——, ——, ——, ——, ——, and J. Kwiatkowski, 2004: A hybrid surface reference technique and its application to the TRMM precipitation radar. *J. Atmos. Oceanic Technol.*, **21**, 1645–1658, doi:10.1175/JTECH1664.1.

Orlandini, S., and I. Morlini, 2000: Artificial neural network estimation of rainfall intensity from radar observations. *J. Geophys. Res.*, **105**, 24 849–24 861, doi:10.1029/2000JD900408.

Qi, Y., J. Zhang, P. Zhang, and Q. Cao, 2013: VPR correction of bright band effects in radar QPEs using polarimetric radar observations. *J. Geophys. Res. Atmos.*, **118**, 3627–3633, doi:10.1002/jgrd.50364.

Rico-Ramirez, M. A., I. D. Cluckie, and D. Han, 2005: Correction of the bright band using dual-polarisation radar. *Atmos. Sci. Lett.*, **6**, 40–46, doi:10.1002/asl.89.

——, ——, G. Shepherd, and A. Pallot, 2007: A high-resolution radar experiment on the island of Jersey. *Meteor. Appl.*, **14**, 117–129, doi:10.1002/met.13.

Roebber, P. J., M. R. Butt, S. J. Reinke, and T. J. Grafenauer, 2007: Real-time forecasting of snowfall using a neural network. *Wea. Forecasting*, **22**, 676–684, doi:10.1175/WAF1000.1.

Schaake, J., A. Henkel, and S. Cong, 2004: Application of PRISM climatologies for hydrologic modeling and forecasting in the western U.S. Preprints, *18th Conf. on Hydrology*, Seattle, WA, Amer. Meteor. Soc., 5.3. [Available online at http://ams.confex.com/ams/pdfpapers/72159.pdf.]

Smyth, T. J., and A. J. Illingworth, 1998: Radar estimates of rainfall rates at the ground in bright band and non-bright band events. *Quart. J. Roy. Meteor. Soc.*, **124**, 2417–2434, doi:10.1002/qj.49712455112.

Wang, Y., J. Zhang, A. V. Ryzhkov, and L. Tang, 2013: C-band polarimetric radar QPE based on specific differential propagation phase for extreme typhoon rainfall. *J. Atmos. Oceanic Technol.*, **30**, 1354–1370, doi:10.1175/JTECH-D-12-00083.1.

Wen, Y., Q. Cao, P.-E. Kirstetter, Y. Hong, J. J. Gourley, J. Zhang, G. Zhang, and B. Yong, 2013: Incorporating NASA spaceborne radar data into NOAA National Mosaic QPE system for improved precipitation measurement: A physically based VPR identification and enhancement method. *J. Hydrometeor.*, **14**, 1293–1307, doi:10.1175/JHM-D-12-0106.1.

Willis, P. T., and A. J. Heymsfield, 1989: Structure of the melting layer in mesoscale convective system stratiform precipitation. *J. Atmos. Sci.*, **46**, 2008–2025, doi:10.1175/1520-0469(1989)046<2008:SOTMLI>2.0.CO;2.

Xu, X., K. Howard, and J. Zhang, 2008: An automatic radar technique for the identification of tropical precipitation. *J. Hydrometeor.*, **9**, 885–902, doi:10.1175/2007JHM954.1.

Zhang, J., and Y. Qi, 2010: A real-time algorithm for the correction of brightband effects in radar-derived QPE. *J. Hydrometeor.*, **11**, 1157–1171, doi:10.1175/2010JHM1201.1.

——, C. Langston, and K. Howard, 2008: Brightband identification based on vertical profiles of reflectivity from the WSR-88D. *J. Atmos. Oceanic Technol.*, **25**, 1859–1872, doi:10.1175/2008JTECHA1039.1.

——, Y. Qi, D. Kingsmill, and K. Howard, 2012: Radar-based quantitative precipitation estimation for the cool season in complex terrain: Case studies from the NOAA Hydrometeorology Testbed. *J. Hydrometeor.*, **13**, 1836–1854, doi:10.1175/JHM-D-11-0145.1.

Zrnić, D. S., and A. V. Ryzhkov, 1996: Advantages of rain measurements using specific differential phase. *J. Atmos. Oceanic Technol.*, **13**, 454–464, doi:10.1175/1520-0426(1996)013<0454:AORMUS>2.0.CO;2.